Mechanistic investigations towards a successful PET with Breslow-Intermediates

Jenny Phan, Julia Rehbein*

Fakultät für Chemie & Pharmazie, Universität Regensburg, Universitätsstrasse 31, 93051 Regenburg

Even under standard catalysis reaction conditions Breslow-intermediates can undergo oxidations that feature NHC stabilized radicals as usually transient intermediates. The idea of making this oxidation step the main reaction pathway and hence harness the ketyl type radicals had previously been proposed by Rehbein et al. Here recent mechanistic studies are summarized to identify the prerequisites to achieve a successful and universally applicable dual NHC-photoredox catalysis that enables the reagent-independent formation of ketyl radicals that may be subsequently trapped by suitable substrates to form new carbon-carbon or carbon heteroatom bonds.

Introduction. NHC-catalysis is a long established form of asymmetric organocatalysis[1] that allows for the umpolung of the inherent electrophilic character of carbonyls.[2] Rather late in regard to the methodological development and mechanistic postulates and associated studies[3,4] the idea evolved that single electron transfer (SET) or proton-coupled electron transfer (PCET) may play a role in the pathways involving the key enaminol structure **EA** (Scheme 1).[5, 6, 7] Detailed studies regarding the origin of EPR-observable open-shell structures (R) and their potential role within the NHC-catalytic cycle let to the conclusion that most likely the Breslow intermediate is the direct precursor of such NHC-stabilized ketyl type radicals (**OH-EA-R**, **EA-dep-R**). Structures like **EA-dep-R** have been proposed in the oxidative NHC-catalysis, but only as an intermediate to the full-two-electron oxidation to feature acyl azolium species.[8] Our interest evolves around the differentiation of the reactivities of the various possible radical structures and their selective formation, i.e. to derive a universal reactivity map under given reaction conditions. As depicted in Scheme 1, one can classify these radicals **R** according to their charge (neutral: **EA-dep-R, OH-PA-R**; cationic: **OH-EA-R**, anionic: **PA-dep-R**) and their ability to accept or donate a hydrogen atom. Hence, quite different chemoselectivity and pathways are expected.

---

[1] R. Kluger, K. Tittmann, *Chem. Rev.* **2008**, *108*, 1797–1833.
[2] R. Breslow, *J. Am. Chem. Soc.* **1958**, *80*, 3719–3726.
[3] M. J. White, F. J. Leeper, *J. Org. Chem.* **2001**, *66*, 5124–5131.
[4] (a) M. Paul, M. Breugst, J.-M. Neudörfl, R. B. Sunoj, A. Berkessel, *J. Am. Chem. Soc.* **2016**, *138*, 5044–5051. (b) A. Berkessel, V. R. Yatham, S. Elfert, J. -M. Neudörfl, *Angew. Chem. Int. Ed.* **2013**, *52*, 11158–11162. (c) A. Berkessel, S. Elfert, V. R. Yatham, J. -M. Neudörfl, N. E. Schlörer **2012**, *51*, 12370–12374. (d) A. Berkessel, S. Elfert, K. Etzenbach-Effers, J. H. Teles, *Angew. Chem. Int. Ed.* **2010**, *49*, 7120–7124.
[5] (a) J. Phan, S.-M. Ruser, K. Zeitler, J. Rehbein *EJOC* **2018**, *2-3*, 557–561. (b) J. Rehbein, S.-M. Ruser, J. Phan *Chem. Sci.* **2015**, ***6***, 6013–6018.
[6] Vianney Regnier. Erik A. Romero, Florian Molton, Rodolphe Jazzar, Guy Bertrand**,** David Martin *J. Am. Chem. Soc.* **2019**, *141*, 2, 1109–1117.
[7] M.-H. Hsieh, G.-T. Huang, J.-S. K. Yu, *J. Org. Chem.* **2018**, *83*, 15202–15209.
[8] J. Guin, S. De Sarkar, S. Grimme, A. Studer *Angew. Chem. Int. Ed.* **2008**, *47*, 8727–8730.

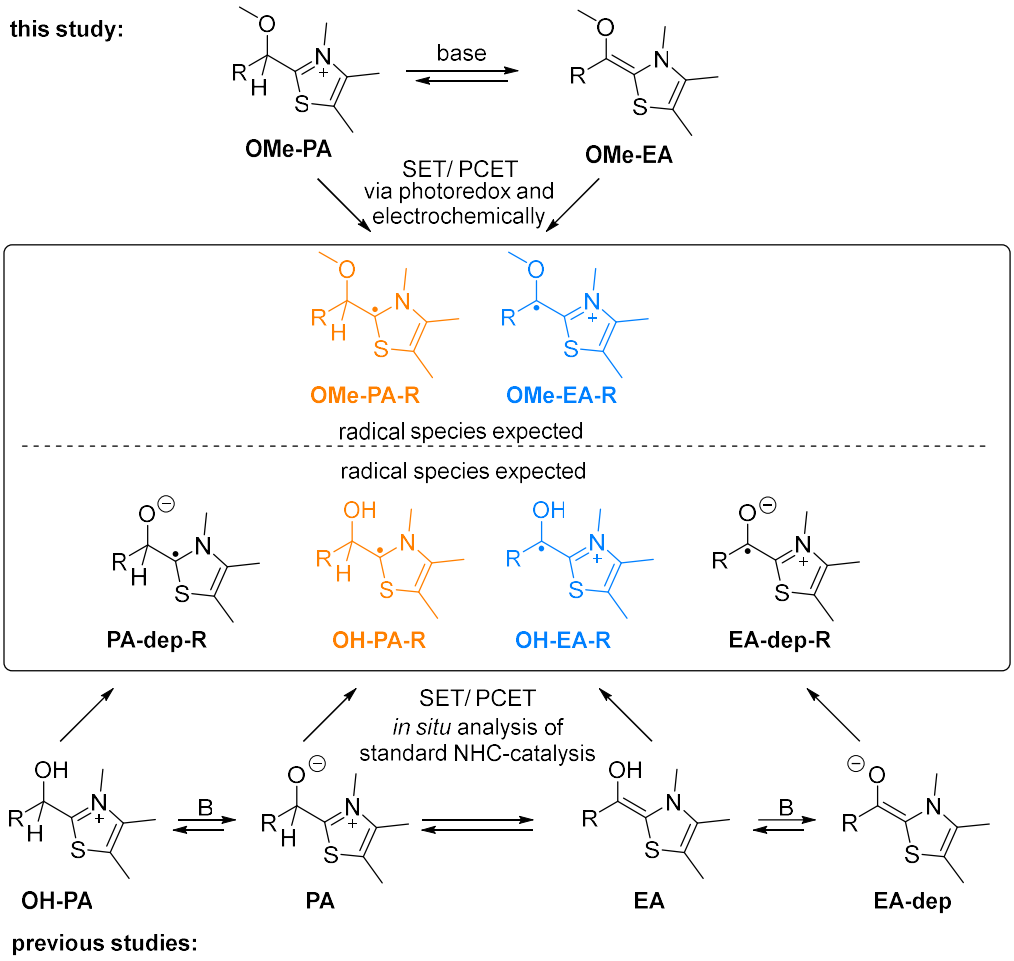

Scheme 1. The key structure of standard NHC-catalysis cycles (bottom part) in the activation of simple aldehyde. The radicals EA-dep-R and OH-EA-R were previously characterized and analyzed regarding their reactivity and their most likely pathway of formation. Highlighted are the similarities between the here studied O-methylated radical species **OMe-PA-R** and **OMe-EA-R** formed via photoredox catalysis and electrochemistry.

Since standard Breslow intermediates (**EA**) and primary adducts (**PA**) are rather fleeting in nature, we decided to make use of the stable *O*-methylated derivates for our mechanistic studies. This approach has the advantages that we have defined starting points for the interaction with the photocatalysts and for electrochemical conversions, it reduces the number of possible acid-base and other pre-equilibria and can test for the broad range of substrate electronics. The following results hence mimic the situation where the Breslow-intermediate is in its neutral state (**EA**) and the primary adduct in its cationic form. These two structures are the ones that are most likely to occur under the widely used protic conditions in standard NHC-catalysis and have also been identified by NMR spectroscopy.[3,4] The synthesis of **OMe-PA** and **OMe-EA** for R = Ph was accomplished as previously described [9,10,11].

These general questions are addressed in the following: Which conditions are needed to have an efficient photoelectron transfer from the excited state photocatalyst (PC*)? Will the photoredox step involving the PC* take place with the enaminol **OMe-EA** selectively or are site-reactions expected with the primary adduct **OMe-PA**? In this regard, how are the **OMe-EA** and the **OMe-PA** linked via redox-

[9] V. Capriati, S. Florio, G. Ingrosso, C. Granito, L. Troisi, *Eur. J. Org. Chem.* **2002**, 478–484.
[10] G. Barletta, A. C. Chung, C. B. Rios, F. Jordan, J. M. Schlegel, *J. Am. Chem. Soc.* **1990**, *112*, 8144–8149.
[11] B. Maji, H. Mayr, *Angew. Chem. Int. Ed.* **2012**, *51*, 10408–10412.

steps (SET vs. PCET). The answers were seeked by a combination of photophysical experiments, like quenching studies and spectro-electro chemistry.

Results & Discussions. Based on previously published CV-data the choice of photoredox catlaysts was made.[5] $[Ru(bpy)_3]^{2+}$ and Eosin Y both have enough redox-potential to access the according SET-derived radicals from primary adduct **OMe-PA** and Breslow-intermediate **OMe-EA**. To avoid complications due to the pH-dependence of the structure of Eosin Y, the disodium salt was used (Na_2Eosin Y).

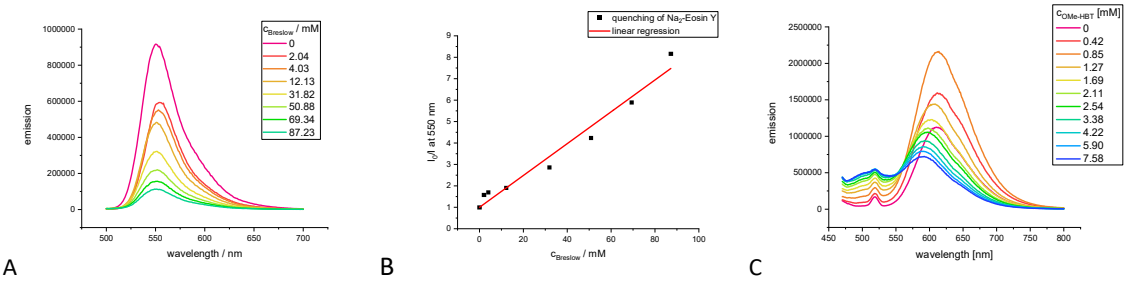

Figure 1. Stern-Vollmer plot (B; I_0 maximal intensity at c_{OMe-EA} = 0; I at $c_{i,\ OMe-EA}$; linear regression with R^2 = 0.99) derived of the fluorescence (550nm) quenching of the Na_2Eosin Y with **OMe-EA** (A). Excitation of Na_2Eosin Y with 480 nm, emission in the 500-700 nm range, slit width 1 nm. C) Same quenching experiment with $[Ru(bpy)_3]Cl_2$.

The quenching of the two (Table 1, Figure 1) photoredox-catalysts with **OMe-PA** and **OMe-EA** with and without sacrificial oxidant or reductant showed that only the Breslow-intermediate **OMe-EA** was able to quench the PC*. This finding was supported by the EPR-spectra taken during irradiation (Figure 2, additional information see SI). In case of **OMe-PA** no radical signal was observed. These results suggest that also under standard catalysis conditions (in protic polar media) with transients **OH-PA** and **EA** being present the selectivity of the redox-steps is highly in favor to take place only with the **EA**. In regard to the choice of photocatalyst the quenching constants suggest that the Na_2Eosin Y is a good lead-structure, with a quenching rate constant being 5.7 x 10^4 times higher than with $[Ru(bpy)_3]Cl_2$ (Table 1).

Table 1. Overview of the quenching experiments with **OMe-EA** using two different PCs and reductive (DIPEA) and oxidative additives (*m*-dinitrobenzene, *m*-DNB).

	$[Ru(bpy)_3]Cl_2$				Na_2Eosin Y			
#	additive	K_{sv} [$L \cdot mol^{-1}$]	k_q / $L \cdot (mol \cdot s)^{-1}$	EPR active	additive	K_{sv} [$L \cdot mol^{-1}$]	k_q / $L \cdot (mol \cdot s)^{-1}$	EPR active
1	DIPEA	1.08	$3.09 \cdot 10^6$	X	DIPEA	0.699	$5.78 \cdot 10^8$	X
2	none	1.08	$4.51 \cdot 10^8$	X	none	74.3	$6.14 \cdot 10^{10}$	X
3	*m*-DNB	55.3	$1.58 \cdot 10^8$	X	*m*-DNB	78.5	$6.49 \cdot 10^{10}$	X

The *in situ* EPR-spectra taken under irradiation of the reaction solution at 530 nm (Na_2Eosin Y)/ 455 nm ($[Ru(bpy)_3]Cl_2$) were used to decide on the possible requirement of sacrificial electron donors or acceptors. As a read-out for the efficiency of the SET process the intensity (double integration of the observed signal) of the EPR-spectra were used to determine when the formation of the ketyl-type radical species is highest (Table 2). In line with the highest quenching rate of the Breslow intermediate **OMe-EA** without any additive and Na_2Eosin Y yielded the highest spin concentrations.

Table 2. Observed changes in the EPR-intensities with the two different PCs and different additive.

#	PC	additive	EPR intensity [a,b]	relative EPR intensity
1	Na_2Eosin Y	none	792	7.0
2	Na_2Eosin Y	Pyridine	521	4.6
3	Na_2Eosin Y	DIPEA	218	1.9
4	Na_2Eosin Y	TEA	175	1.5
5	Na_2Eosin Y	$K_2S_2O_8$	343	3.0
6	$[Ru(bpy)_3]Cl_2$	Pyridine	430	3.8
7	$[Ru(bpy)_3]Cl_2$	$K_2S_2O_8$	113	1.0 (ref.)

[a] after 10 min of irradiation. [b] based on integrated area (double integration of observed signal)

In presence of additives not only the quenching rates of PC* are partially lowered (amines) but also the radical concentrations in comparison to the reaction solutions without any additives. The latter observation can either be explained by three different scenarios: First, the competition between additive and **OMe-PA** in the quenching of the PC*. Second, by an onwards reaction of the formed **OMe-PA-R** with the additive to a closed shell species. Third, by an effective pre-complexation of PC or **OMe-EA** prior to irradiation which is suspended or triggered by the presence of an additive.

Table 3. Comparison of the quenching rates k_q of the additives and **OMe-PA** in degassed THF.

#	PC	c in THF [µM]	quencher	c in THF [M]	K_{SV} [L/mol] x 10^{-4}	$k_F+k_{nr} = 1/\tau$ [1/s]	k_q [L/mol/s] x 10^8	$k_{q,rel}$
1		10	DIPEA	neat	8	826446281	6.68	1
2	Na_2Eosin-Y	10	mDNB	1.2	600	826446281	496	74
3		9	**OMe-EA**	1.2	773	826446281	639	96
7		8	DIPEA	neat	11	2857142	0.03	1
8	$Ru(bipy)_3Cl_2$	11	mDNB	1.2	695	2857142	20	667
9		8	**OMe-EA**	1.3	700	2857142	20	667

Based on the independent quenching rates measured for the two PCs by the different additives in comparison to **OMe-EA** (Table 3) the first hypothesis may be applicable for the oxidizing, but not for the reducing additives. In case of the reducable additives (*m*-DNB, $K_2S_2O_8$) the quenching rates are very similar to the ones of **OMe-EA** and hence the observation of unchanged quenching constants but lower amounts of **OMe-EA-R** may be explained by a competition for PC* (Table 3, Entries 2, 3, 8, 9). In case of the amines the situation is somewhat different. **OMe-EA** is 96 (Na_2Eosin Y) to 667 ($[Ru(bpy)_3]Cl_2$) times faster than the amine in quenching the PC*. Still the quenching rate of PC* in the reaction solution is diminished for both PCs as well as the concentration of **OMe-EA-R** (Table 2).

The above mentioned hypothesis of assembly formations of the three components in different permutations like PC•**OMe-EA**, PC•PC or **OMe-EA**•amine was pursued first. Although Brønsted acid-base interactions with **OMe-PA** and the amine prior to irradiation seem unlikely, UV-vis spectra of **OMe-EA** recorded as a function of c_{DIPEA} and by the quenching studies of the **OMe-EA** fluorescence (Figure 2). As both, UV-vis absorption and fluorescence are continuously enhanced with rising base concentrations an assembly formation already in the electronic ground state between these two

molecular species is likely. This type of assembly is deemed to be undesired as it apparently leads to a less efficient quenching of PC*.

That a similar assembly between PC and **OMe-EA** prior to the SET step especially between $[Ru(bpy)_3]Cl_2$ and **OMe-EA** is a likely option can be derived from the quenching experiments shown above (Figure 1B). The shift of the wavelength and initial increase of the fluorescence upon continuous addition of **OMe-EA** indicate a molecular association step of both structures. Such an assembly might allow for a very efficient PET. Therefore, the efficiency of this interaction between PC and **OMe-EA** was studied further by determining the possibility of a dark redox-reaction between PC and **OMe-EA**, that would require and hence prove the pre-association of both structures independently of the Stern-Volmer quenching studies (Figure 3B-D).

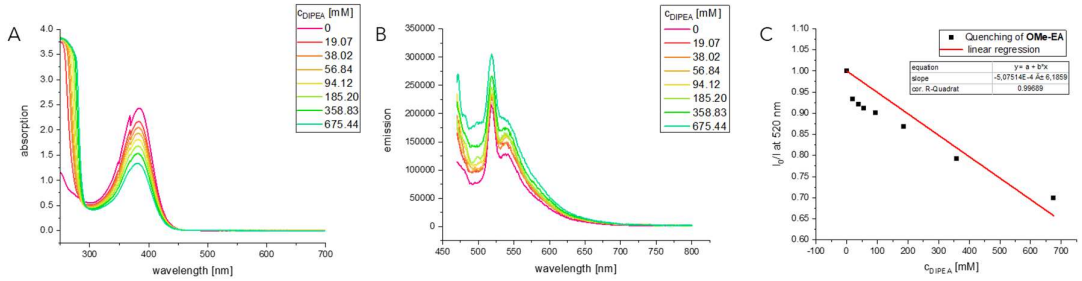

Figure 2. A: UV-vis absorption spectra of **OMe-EA** during the titration with DIPEA. The absorption maximum increases continuously with the base concentration indicating the complex formation in the electronic ground state. B: Fluorescence quenching of **OMe-EA** with DIPEA; irradiation at 450 nm (slit-width: 6 nm), emission: 470−800 nm (slid width: 6 nm) C: associated Stern-Volmer plot to B.

In case of both PCs the radical concentration in presence of **OMe-EA** and pyridine or $K_2S_2O_8$ is significantly above zero even without light (Figure 3B-D). In case of the oxidative additives the oxidation of the **OMe-EA** may take place and was also shown by the EPR-spectra of the control experiments. In case of the amines this rational is not applicable. However, further control experiments by EPR spectroscopy could show that it is not the PC itself or its interaction with pyridine (see SI) or an interaction between pyridine and **OMe-EA** that gave rise to the observed dark reaction. This leaves a thermally activated SET process within an assembly of **OMe-EA** and PC as the only rational.

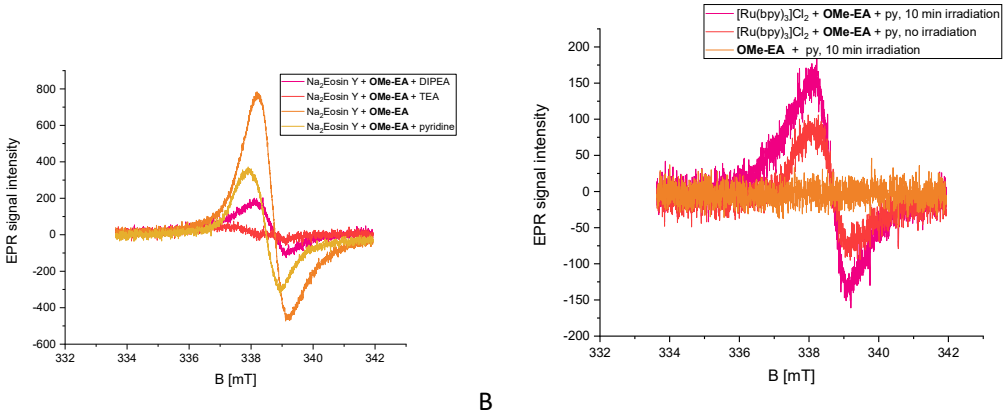

A B

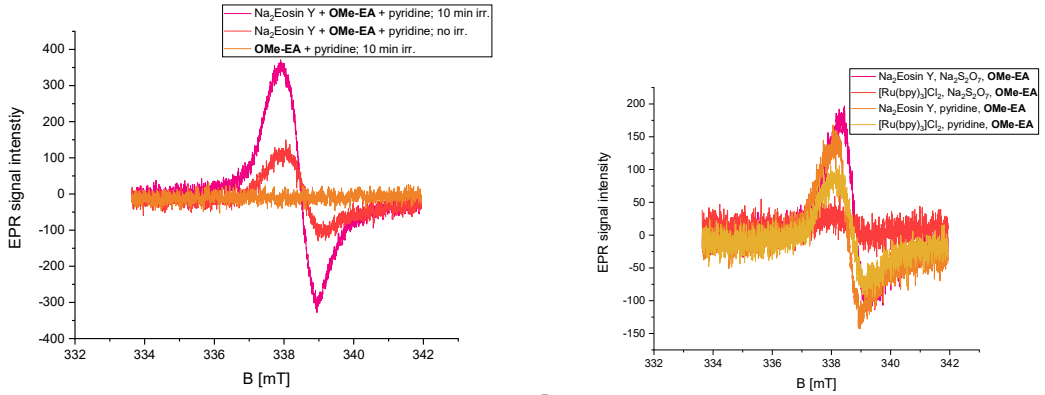

C D

Figure 3. EPR monitoring of the reaction solutions (**OMe-PA** , PC (5 mol%), 2 eq or no additive in degassed THF) during irradiation at t =10 min: A) with Na_2Eosin Y (λ_{irr} = 530 nm) and different amine bases (2 eq) ; B) comparison with $[Ru(bpy)_3]_2Cl_2$ and 2 eq pyridine (λ_{irr} = 455 nm) C) Na_2Eosin Y in presence of pyridine (2 eq) without irradiation. D) Comparison of dark background reaction in dependence of PC and **OMe-EA-R**. *measurement conditions: mean field 337.784 mT, width: 8.305 mT, µwave power: 10 mW, t: 30 s, amplitude of modulation: 0.7 mT, reciever gain: 10 dB.*

With this assembly in place the hypothesis of the amine acting as a reactant for **OMe-EA-R** is not ruled out yet. Therefore, the concentration of **OMe-EA-R** was measured by EPR in dependence on the amine structure. Since reactions with TEA and also DIPEA led to a stronger loss in radical concentration than pyridine (Figure 2A) a HAT pathway from amine to **OMe-EA-R** seems most likely. Consequences for an attempted dual catalysis approach would be to avoid amine bases that feature HAT reactivity, since these can apparently transform the **OMe-EA-R** derived from the PET process of the **OMe-EA** back into the photoredox inactive primary adduct **OMe-PA**. The direct HAT-relationship between the protected Breslow- and primary adduct was shown in an independent set of spectro-electrochemical experiments (Figure 3, discussion vide infra).

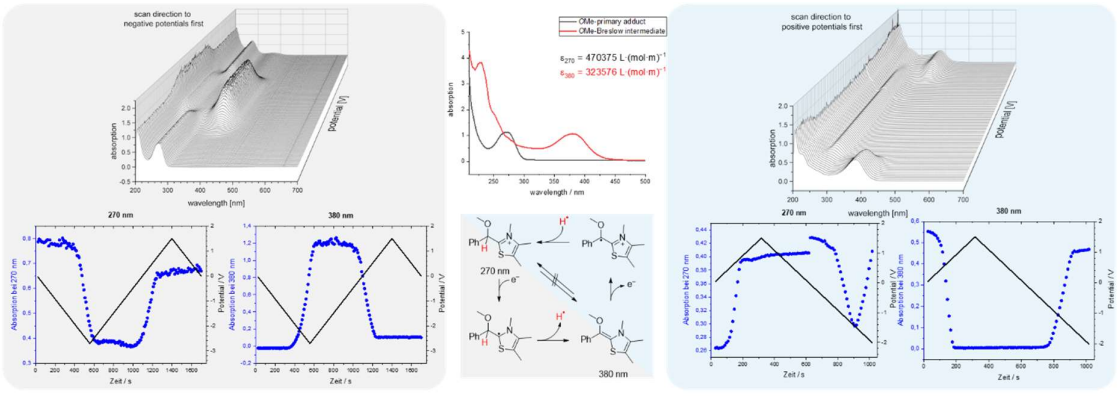

Figure 3. Summary of the spectro-electrochemical studies of **OMe-PA** (left) and **OMe-EA** (right) in THF using the UV-vis absorption as a read out to identify the resulting intermediates. Clearly there is a PCET interconnection under these electrochemical conditions between **OMe-PA** and **OMe-EA** that most likely is mimicked under photoredox-catalytic conditions in presence of HAT-donors/acceptors.

To elucidate further if the hypothesis of a direct transformation of **OMe-EA** to **OMe-PA** and vice versa via a PCET is possible spectro-electrochemical experiments were conducted. Hereby, the UV-vis spectra were record whilst driving the potential of the electrochemical cell until oxidation or reduction peak potentials of **OMe-PA** and **OMe-EA** were reached (as determined previously by CV). The UV-vis spectra of **OMe-PA** and **OMe-EA** have characteristic absorption bands that allow for an unambiguous identification of these structures (Figure 4, center).

Starting with the **OMe-PA** the scan direction was first going towards negative potentials and then reversed. Opposite scan-directions were used to study the UV-vis spectra of the electrochemically derived intermediates of **OMe-EA**. This choice of scan directions resulted from the previously conducted cyclovoltammetry measurements (see SI) and were corroborated by the observation that only then changes in the UV-vis spectra are observed (Figure 4, top).

The UV-spectra recorded in dependence of the potential indicate that the **OMe-PA** will become – after a SET reduction – a potent hydrogen atom donor, leading to the **OMe-EA** after a HAT step. In this electrochemical experiment the only HAT-acceptor is the solvent. But one can envision substrates that can be reduced via HAT under these electrochemical conditions. The inverted behavior is observed for the **OMe-EA**. After a SET oxidation the resulting **OMe-EA-R** will quickly release a hydrogen atom to return to the closed shell **OMe-OPA**.

Conclusions. In this study the interconversion via PCET between **OMe-PA** and **OMe-EA**, i.e. the stable derivatives of the primary adduct (cationic form) and the Breslow intermediate (neutral form) have been shown by spectro-electrochemistry. Under photoredox catalysis conditions only the enaminol **OMe-EA** was able to quench the excited state of the photocatalyst (PC), raising the expectation that the in a dual catalysis approach the PET will be selective for **OMe-EA**. The PET step produced an EPR signal that has been previously characterized to be the radical from a SET oxidation step of **OMe-EA**. The reductive quench cycle hence is in operation. Combined quenching and EPR studies suggest, that amine additives that can undergo hydrogen atom transfer (HAT) are counterproductive as these return the **OMe-EA-R** into the unreactive **OMe-PA**. Also, experimental evidence has been found for a productive (SET reactive) ground state assembly between PC and **OMe-EA** as well as a counter-productive amine-**OMe-EA** complex. Based on these fundamental mechanistic insights synthetic applications like the dual NHC-photoredox catalysis targeting the Breslow intermediate as the reductant for the photocatalyst are currently worked on and will be published in due course.

Supporting Information

Mechanistic investigations towards a successful PET with Breslow-Intermediates

Jenny Phan, Julia Rehbein*

Fakultät für Chemie & Pharmazie, Universität Regensburg, Universitätsstrasse 31, 93051 Regenburg

Content of SI

EPR spectroscopy

For the EPR measurements two spectrometers were used, a Bruker Elexsys E500 CW and a Magnettech MiniScope MS400. All samples were degassed for several cycles via *freeze-pump-thaw* and transferred into N2-flushed quartz-tubes (outer diameter: 4 mm, inner diameter: 3.5 mm) or into quartz tubes with PTFE-screw cap (outer diameter: 4 mm, inner diameter: 3.2 mm. For simultaneous irradiation, a DC Mini Jolly LED with 20 W maximum power has been used. Simulations of EPR-spectra was done with WinSim (Version 0.98).[12]

Base line correction was manually applied by analyzing the raw data in Origin® using the weighted end-point method.[13] To allow for a better comparison for spectra measured at different µwave powers equation 1 was used (shown for a referencing to 2.631 mW).

$$intensity_{\mathrm{new}} = \frac{intensity_{\mathrm{old}}}{conversion\ factor} \qquad \textbf{Eq. 1}$$

Conversion factor: $\left(\frac{\mu wave\ power}{2.631\ \mathrm{mW}}\right)^{0.5}$

[12] D. R. Duling, *J. Magn. Reson., Series B* **1994**, *104*, 105–110, DOI: 10.1006/jmrb.1994.1062.

[13] *Origin 2017G*, OriginLab Corporation, Northampton, MA, USA

EPR studies: additional material of control experiments

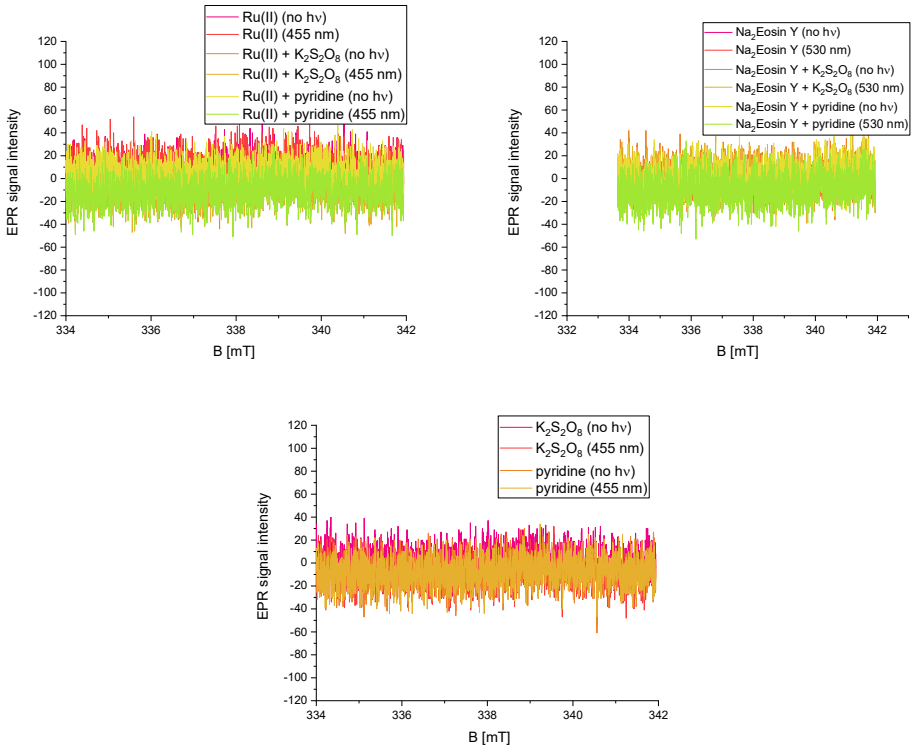

Figure SI-4. EPR-spectra of the reaction solutions containing photocatalyst $[Ru(bpy)_3]Cl_2$ or Na_2Eosin Y (5−10 mol%) with and without additives $K_2S_2O_8$ or pyridine (2 eq.). The sample were measured with (455/530 nm for 10 min) and without irradiation. Measurement conditions: mean field: 337.784 mT, width: 8.305 mT, µwave power: 10 mW, time: 30 s, modulation amplitude: 0.7 mT, receiver gain: 10 dB.

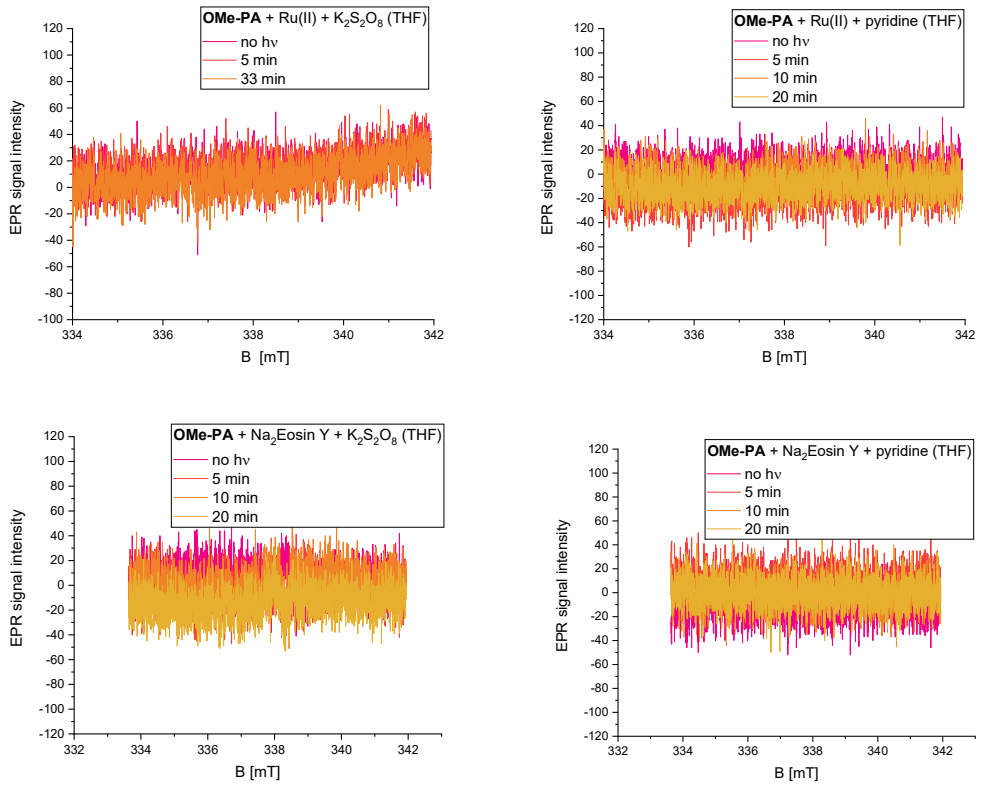

Figure SI-5. EPR-spectra of the reaction solutions containing **OMe-PA** (0.05 M in THF), photocatalyst $[Ru(bpy)_3]Cl_2$ or Eosin Y (5–10 mol%) and $K_2S_2O_8$ or pyridine (2 eq.). The sample were measured with (455/530 nm) and without irradiation. Measurement conditions: mean field: 337.784 mT, width: 8.305 mT, µwave power: 10 mW, time: 30 s, modulation amplitude: 0.7 mT, receiver gain: 10 dB.

In this set of experiments (Figure SI-2) one clearly sees that neither with the transition metal nor with the organic dye the primary adduct **OMe-PA** gave rise to an EPR signal under the conditions without additive or in presence of pyridine. For Na_2Eosin Y the typical radical signature of the SET of the Eosin (center 339 mT) derived radical emerges in presence of $K_2S_2O_8$ under prolonged (t ≥ 20 min) irradiation (for comparison of the see Goux et al.[14]). However, the radical concentration is significantly lower than observed with **OMe-EA**.

Fluorescence spectroscopy

Fluorescence spectra were recorded on a HORIBA FluoroMax®-4 spectro fluorometer in a florescence cell of *d* = 10 mm. The quenching constants were calculated using Eq.2.[15] The Stern-Volmer constant was derived of the slope (linear fitting) from the Stern-Volmer plot.

$$k_q = \frac{K_{SV}}{\tau} \qquad \textbf{Eq. 2}$$

[14] A. Goux, T. Pauport, D. Lincot, L. Dunsch *ChemPhysChem* **2007**, *8*, 926–931.

[15] J. R. Lakowicz, *Principles of Fluorescence Spectroscopy,* 3. Aufl., Springer Science+Business Media, Boston, **2006**.

k_q quenching constant [L·(mol·s)$^{-1}$]

K_{SV} Stern-Volmer constant [L·mol^{-1}]

τ lifetime of fluorophore [s]

$[Ru(bpy)_3]^{2+}$: 350 ns; Eosin Y: 1.21 ns)[99]

Stern-Volmer quenching studies: raw data and analyses

Table SI-4. Table of the changes in intensities at 550 nm from the emission spectra of **Na_2Eosin Y** during titration with **OMe-EA**. Stern-Volmer plot is shown in the main text.

$C_{OMe\text{-}EA}$ / mM	I at 550 nm	I_0/I
0	916640	1
2.04	579670	1.581
4.03	540600	1.696
12.13	479460	1.912
31.82	320650	2.859
50.88	216370	4.236
69.34	155730	5.886
87.23	112370	8.157

Table SI-5. Table of the changes in intensities at 610 nm from the emission spectra of **$[Ru(bpy)_3]Cl_2$** during titration with **OMe-EA**. Potted raw data (also shown in the main text) and Stern-Volmer graph are shown below (Figure SI-3).

$C_{OMe\text{-}PA}$ / mM	I bei 610 nm	I_0/I
0	1124700	1
0.42	1580890	0.711
0.85	2150290	0.523
1.27	1431900	0.785
1.69	1195680	0.941
2.11	1052990	1.068
2.54	983050	1.144
3.38	847170	1.328
4.22	755670	1.488
5.90	677990	1.659
7.58	621610	1.809

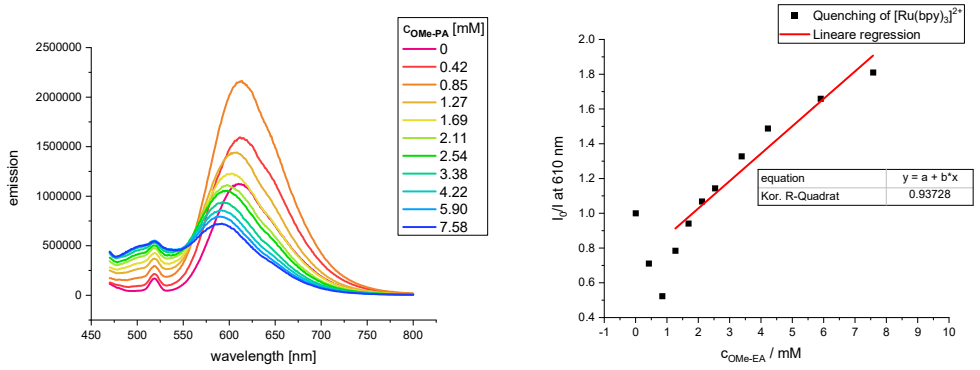

Figure SI-6. Left: Quenching of the fluorescence of **[Ru(bpy)$_3$]Cl$_2$** as a function of $c_{OMe\text{-}EA}$ in THF. Irradiation at 450 nm (slid width: 6 nm), emission: 470–800 nm (slid width: 6 nm). Right: Stern-Volmer diagram fitted with a linear function (R^2 = 0.94) yielding K value as shown in main text.

Table SI-6. Table of the changes in intensities at 610 nm from the emission spectra of **[Ru(bpy)$_3$]Cl$_2$** during titration with **DIPEA**. Potted raw data and Stern-Volmer graph are shown below (Figure SI-4).

c_{DIPEA} [mM]	I at 610 nm	I_0/I
0	1084910	1
19.07	1033060	1.050
56.84	979200	1.108
130.91	906010	1.197
273.39	794270	1.366
441.64	718950	1.509
599.83	678000	1.600
748.86	608230	1.784
889.49	556090	1.951
1022.42	519310	2.089
1148.25	477520	2.272

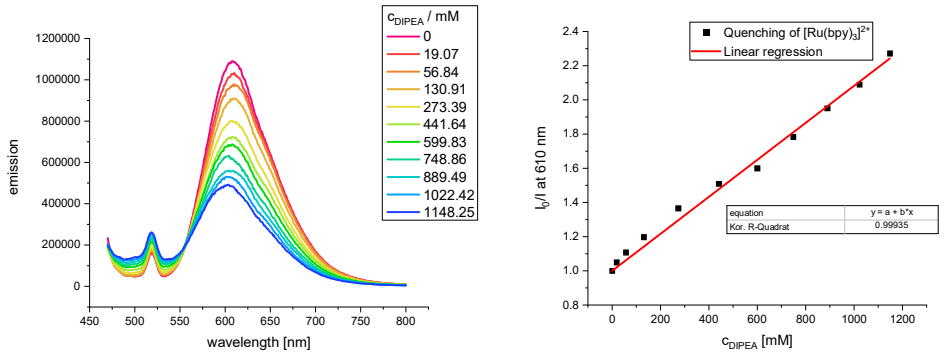

Figure SI-7. Left: Quenching of the fluorescence of **[Ru(bpy)$_3$]Cl$_2$** as a function of c_{DIPEA} in THF. Irradiation at 450 nm (slid width: 6 nm), emission: 470–800 nm (slid width: 6 nm). Right: Stern-Volmer diagram fitted with a linear function (R^2 = 0.99) yielding K value as shown in main text.

Table SI-7. Table of the changes in intensities at 612 nm from the emission spectra of **[Ru(bpy)$_3$]Cl$_2$** during titration with **m-DNB**. Potted raw data and Stern-Volmer graph are shown below (Figure SI-5).

c_{mDNB} [mM]	I at 612 nm	I_0/I
0	1284080	1
0.40	1458470	0.880
0.80	1369650	0.938
1.20	1310570	0.980
1.60	1271340	1.010
2.40	1172310	1.095
3.19	1109070	1.158
3.99	1038650	1.236
5.97	946140	1.357
9.92	811960	1.581
19.67	656990	1.954

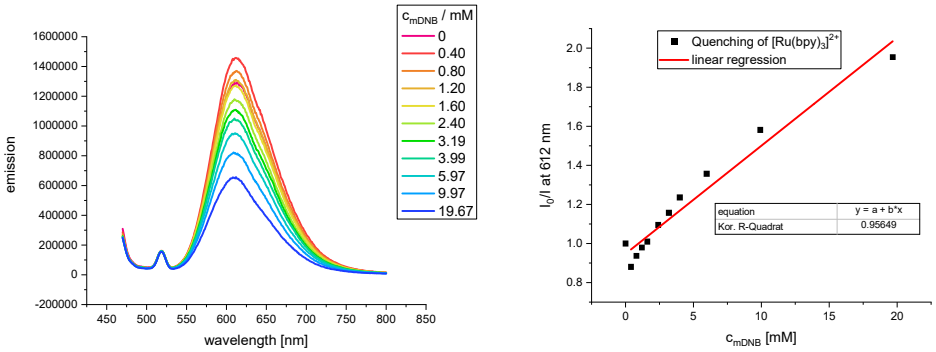

Figure SI-8. Left: Quenching of the fluorescence of **[Ru(bpy)$_3$]Cl$_2$** as a function of c_{mDNB} in THF. Irradiation at 450 nm (slid width: 6 nm), emission: 470–800 nm (slid width: 6 nm). Right: Stern-Volmer diagram fitted with a linear function (R^2 = 0.96) yielding K value as shown in main text.

Table SI-8. Table of the changes in intensities at 545 nm from the emission spectra of **Na_2-Eosin Y** during titration with **DIPEA**. Potted raw data and Stern-Volmer graph are shown below (Figure SI-6).

c_{DIPEA} [mM]	I at 545 nm	I_0/I
0	906930	1
9.55	1460220	0.621
19.07	1620270	0.560
28.56	1655260	0.548
38.02	1683620	0.539
47.45	1682060	0.539
56.84	1693540	0,536
75.54	1666230	0.544
94.12	1651330	0.549
185.2	1510030	0.601
273.39	1359400	0.667
358.83	1243100	0.730
441.64	1141240	0.795
521.93	1054480	0.860

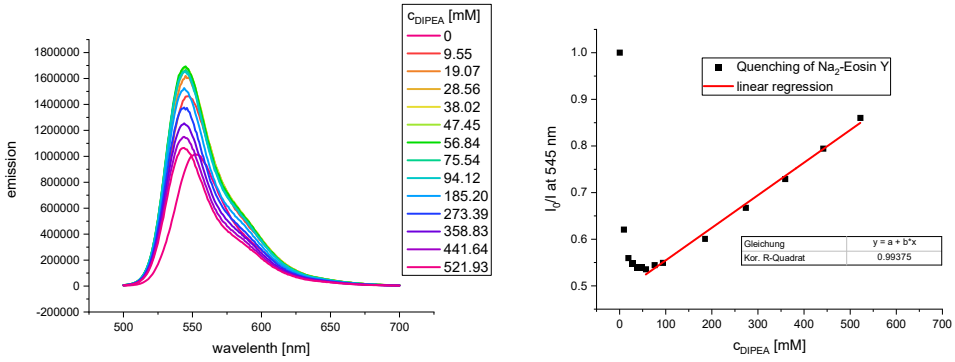

Figure SI-9. Left: Quenching of the fluorescence of **Na_2-Eosin Y** as a function of c_{mDIPEA} in THF. Irradiation at 480 nm (slid width: 6 nm), emission: 500–700 nm (slid width: 1 nm). Right: Stern-Volmer diagram fitted with a linear function (R^2 = 0.99) yielding K value as shown in main text. Interestingly the fluorescence increases and shifts on the first titration points. This is quite similar to the results with $[Ru(bipy)_3]Cl_2$. So in both cases there seems to be an assembly of the PC (in this case with itself) that is broken up by the addition of the amine base or the quencher in general.

Table SI-9. Table of the changes in intensities at 552 nm from the emission spectra of **Na_2-Eosin Y** during titration with **m-DNB**. Potted raw data and Stern-Volmer graph are shown below (Figure SI-7).

c_{mDNB} / mM	I bei 552 nm	I_0/I
0	881670	1
2.00	790330	1.116
3.99	704400	1.252
5.97	638700	1.380
7.95	565200	1.560
9.92	511460	1.724
11.88	460550	1.914
13.84	416830	2.115
15.79	382160	2.307
19.67	341840	2.579

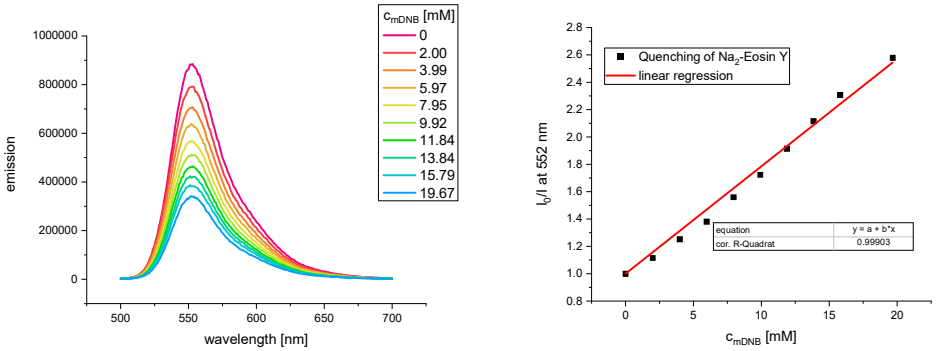

Figure SI-10. Left: Quenching of the fluorescence of **Na_2-Eosin Y** as a function of c_{mDNB} in THF. Irradiation at 480 nm (slid width: 6 nm), emission: 500–700 nm (slid width: 1 nm). Right: Stern-Volmer diagram fitted with a linear function (R^2 = 0.99) yielding K value as shown in main text.

Table SI-10. Table of the changes in intensities at 520 nm from the emission spectra of **OMe-EA** during titration with **DIPEA**. Potted raw data and Stern-Volmer graph are shown in the main text.

C_{DIPEA} [mM]	I at 520 nm	I_0/I
0	209350	1
19.07	224470	0.933
38.02	227160	0.922
56.84	229720	0.911
94.12	232610	0.900
185.2	241090	0.868
358.83	264450	0.792
675.44	299610	0.699

NMR spectroscopy

NMR spectra were recorded at a Bruker Fourier HD 300, Avance 300 and Avance III HD 400. Chemical shifts δ are reported in ppm and are relative to the the signal of Tetramethylsilan (^{1}H NMR: 0.00 ppm) or the non-deuterated traces of the NMR solvent (Chloroform-*d* (^{1}H-NMR: 7.26 ppm, ^{13}C-NMR: 77.16 ppm). Multiplicities of the singnals are reported as s = singulet, d = dublet, t = triplet, q = quartet, quint = quintet, dd = doublet of doublet, dt = doublet of triplet, td = triplet of doublet, qd = quartet of doublet, m = multiplet, br = broad signal.

Synthesis of the **OMe-EA** and **OMe-PA** have been reported previously by us (see main text, citations 5a,b) In the following the ^{1}H and ^{13}C spectra are provided to ensure identity.

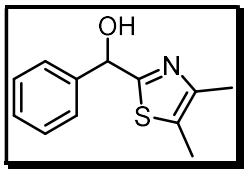

1
$C_{12}H_{13}NOS$
219.30 g·mol^{-1}

Yield	white solid (7.8 g, 36 mmol, 73 %).
^{1}H NMR	(400 MHz, $CDCl_3$): δ = 7.39−7.37 (m, 2H, 2×H_{ar}), 7.28−7.17 (m, 3H, 3×H_{ar}), 5.85 (s, 1H, C**H**), 4.59 (br s, 1H, O**H**), 2.18 (s, 3H, C**H**$_3$), 2.16 (s, 3H, C**H**$_3$).
^{13}C NMR	(100 MHz, $CDCl_3$): δ = 169.9 (N**C**S), 147.5 (C_{ar}), 141.9 (C_{ar}), 128.6 (C_{ar}), 128.3 (C_{ar}), 127.2 (C_{ar}), 126.6 (C_{ar}), 73.4 (**C**H), 14.6 (**C**H$_3$), 11.4 (**C**H$_3$).

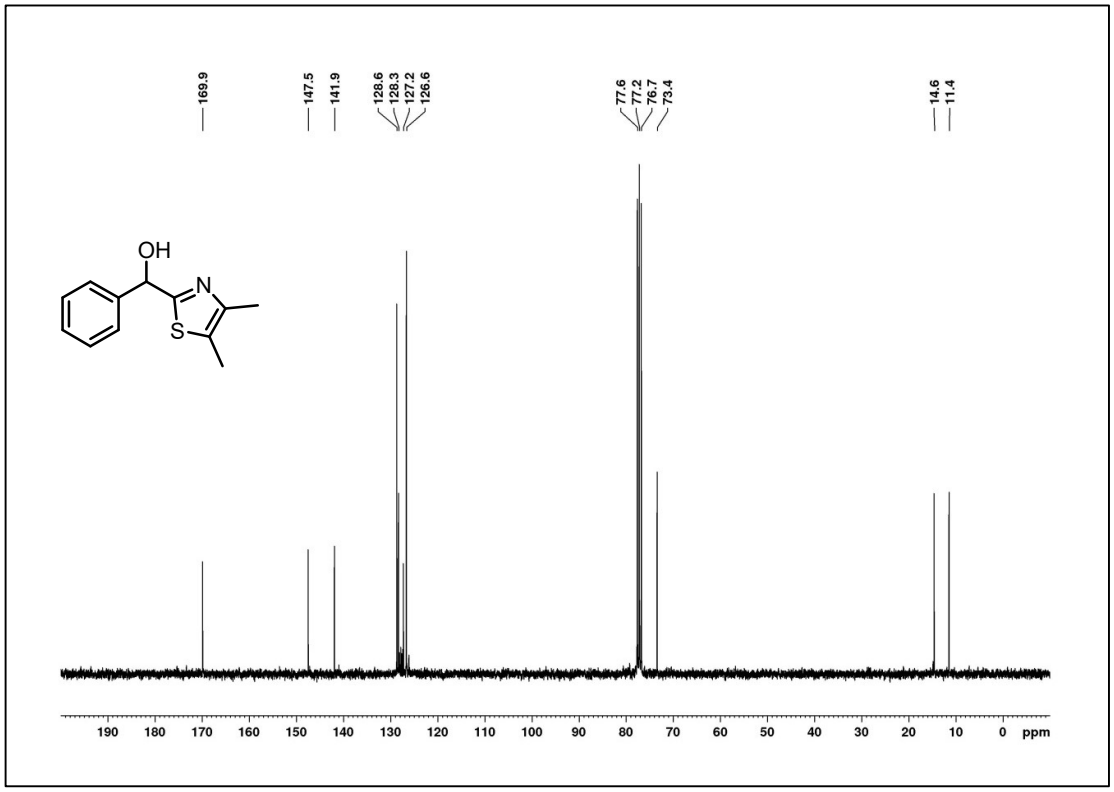

Figure SI-11. ^{13}C-NMR-Spektrum von **1** in $CDCl_3$ (75 MHz).

2
$C_{13}H_{15}NOS$
233.33 g·mol^{-1}

Yield	yellow liquid (7.9 g, 34 mmol, 97 %).
^{1}H NMR	(400 MHz, $CDCl_3$): δ = 7.44−7.42 (m, 2H, H_{ar}), 7.34−7.23 (m, 3H, H_{ar}), 3.42 (s, 3H, OC**H**$_3$), 2.26 (s, 6H, 2×C**H**$_3$).
^{13}C NMR	(100 MHz, $CDCl_3$): δ = 167.6 (N**C**S), 147.8 (C_{ar}), 140.0 (C_{ar}), 128.7 (C_{ar}), 128.3 (C_{ar}), 127.2 (C_{ar}), 126.9 (C_{ar}), 83.2 (**C**H), 57.5 (O**C**H$_3$), 14.8 (**C**H$_3$), 11.4 (**C**H$_3$).

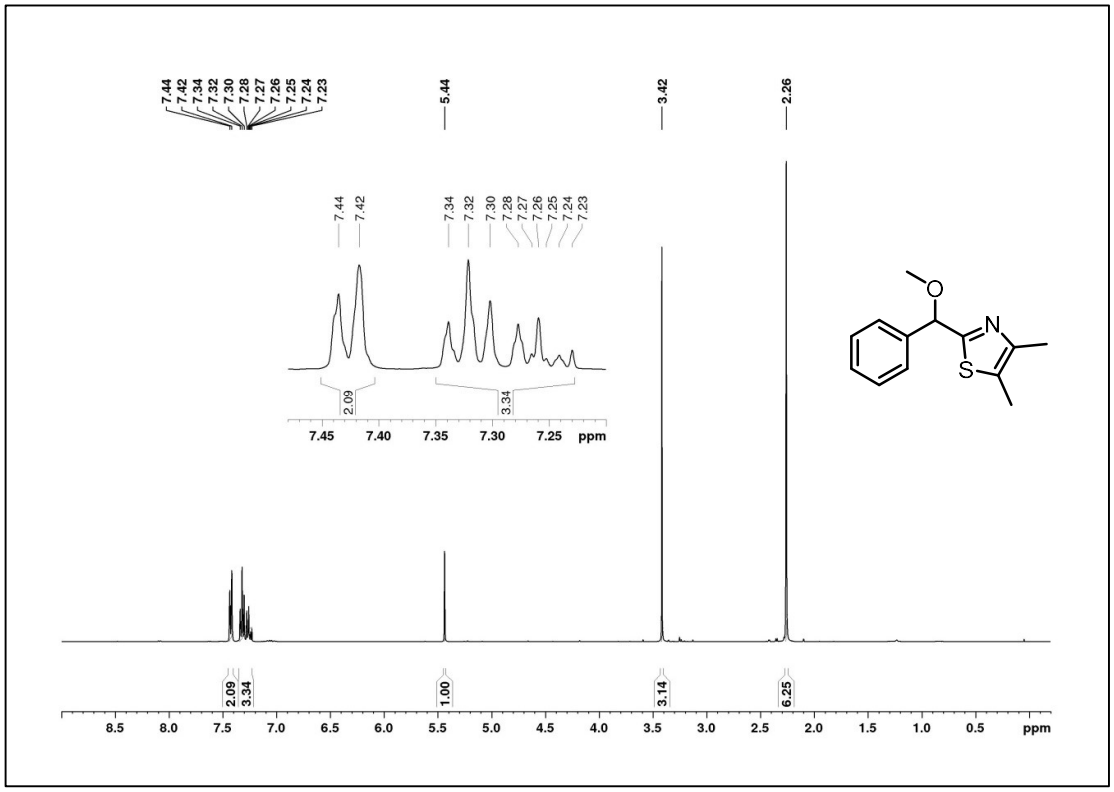

Figure SI-12. ^{1}H NMR of **2** in $CDCl_3$ (400 MHz).

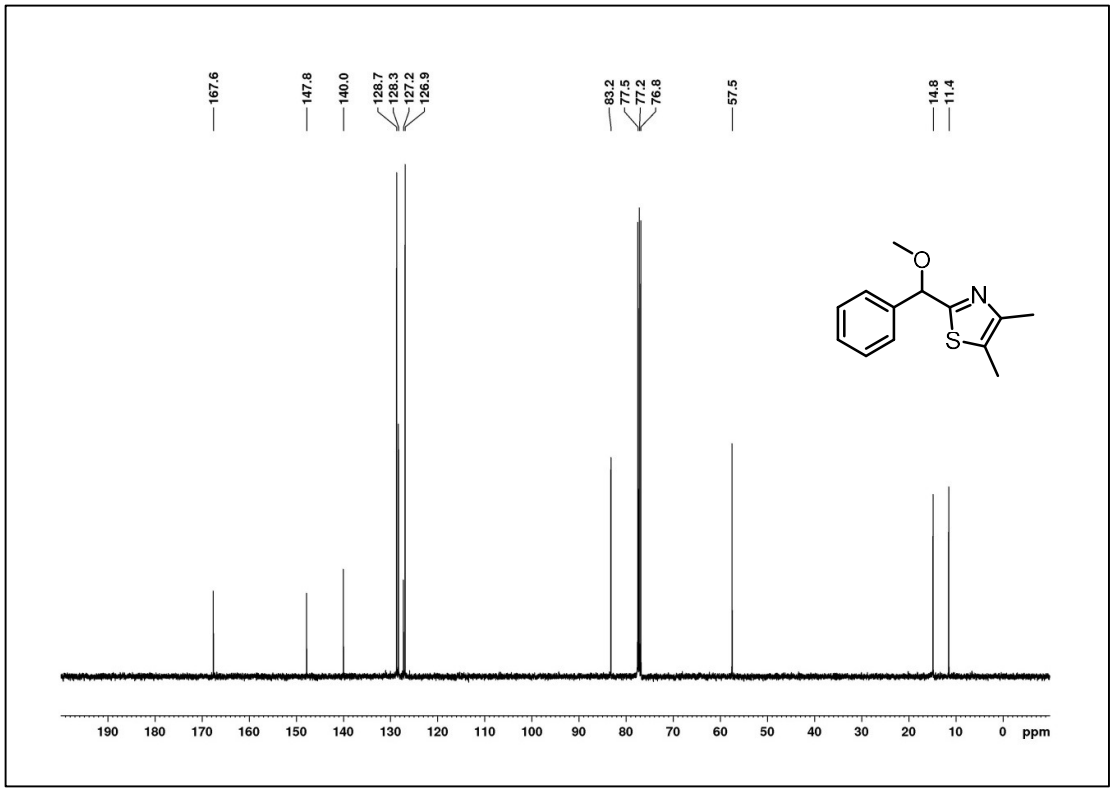

Figure SI-13. ^{13}C NMR of **2** in $CDCl_3$ (100 MHz).

OMe-PA
$C_{14}H_{18}BF_4NOS$
335.17 g·mol^{-1}

Yield oil (11.3 g, 34 mmol, quantitative).

^{1}H NMR (400 MHz, $CDCl_3$): δ = 7.43 (s, 5H, 5×H_{ar}), 5.90 (s, 1H, C**H**), 3.81 (s, 3H, OC**H**$_3$), 3.44 (s, 3H, NC**H**$_3$), 2.44 (s, 3H, C**H**$_3$), 2.38 (s, 3H, C**H**$_3$).

^{13}C NMR (100 MHz, $CDCl_3$): δ = 172.2 (N**C**S), 144.0 (C_{ar}), 134.1 (C_{ar}), 130.8 (C_{ar}), 130.5 (C_{ar}), 129.6 (C_{ar}), 128.4 (C_{ar}), 78.8 (**C**H), 57.7 (N**C**H$_3$), 38.3 (O**C**H$_3$), 12.3 (**C**H$_3$), 12.0 (**C**H$_3$).

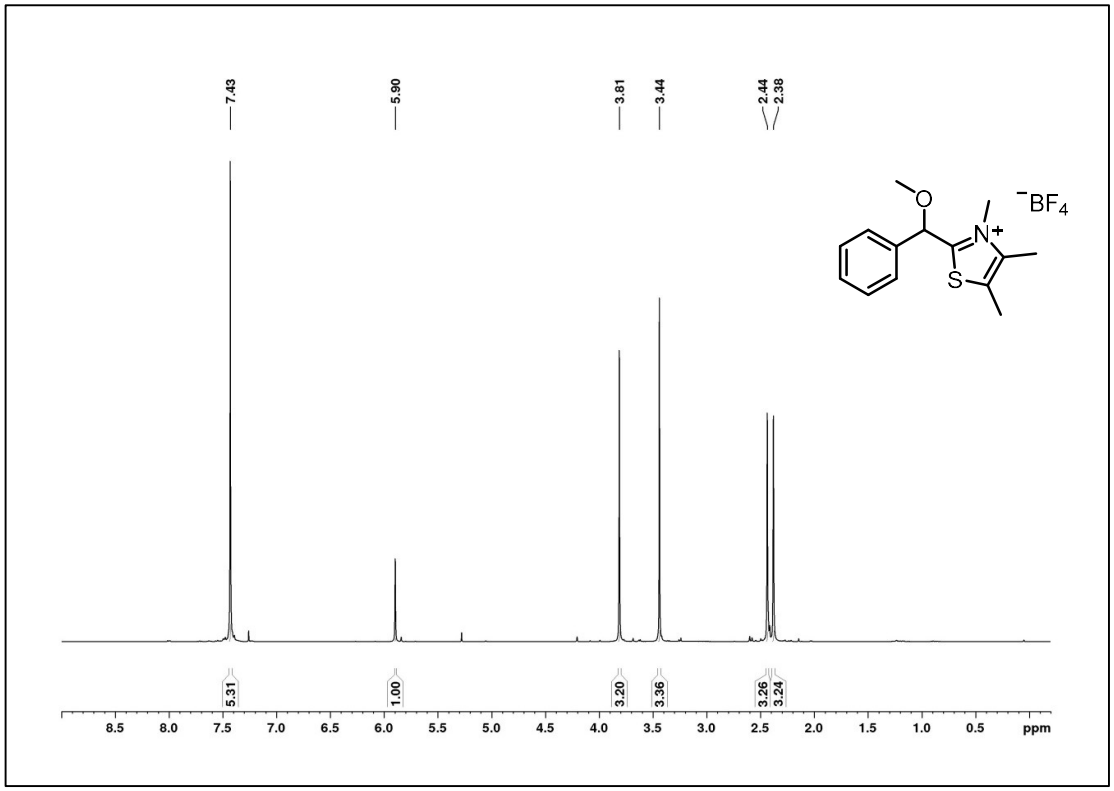

Figure SI-14. ^{1}H NMR of **OMe-PA** in $CDCl_3$ (400 MHz).

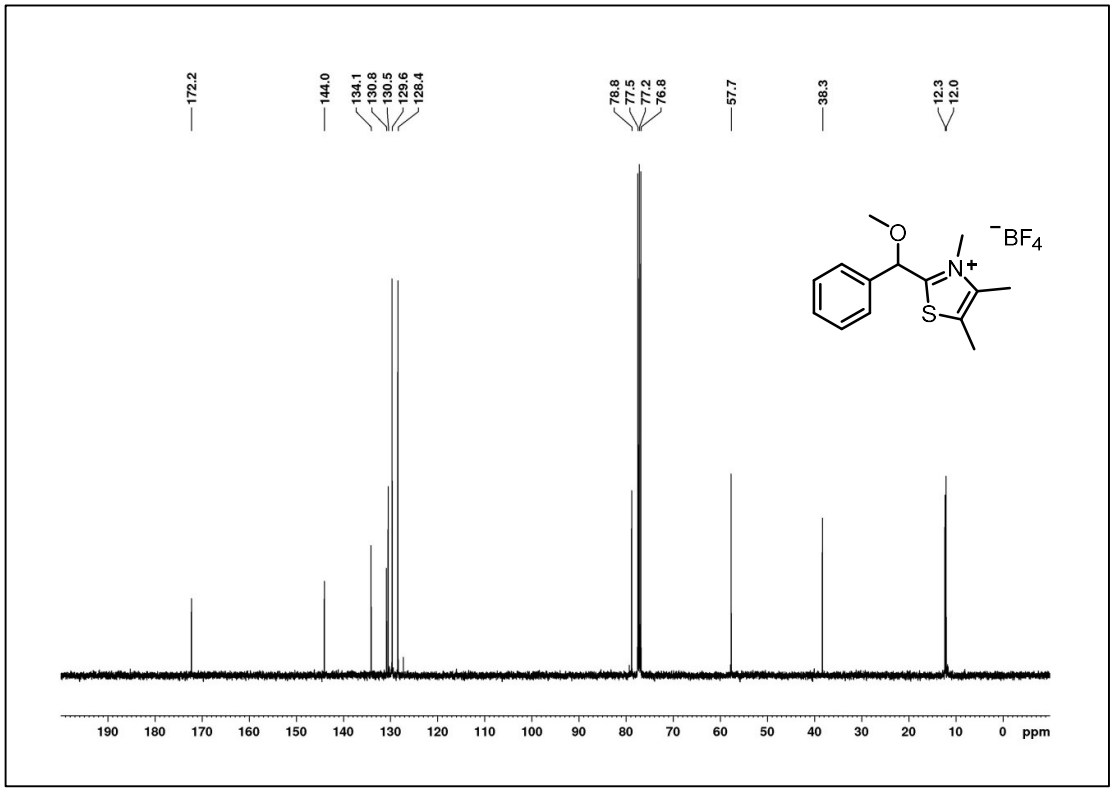

Figure SI-15. ^{13}C NMR of **OMe-PA** in $CDCl_3$ (100 MHz).

OMe-EA
$C_{14}H_{17}NOS$
247.36 g·mol^{-1}

Yield oil (11.3 g, 34 mmol, quantitative).

^{1}H NMR (400 MHz, $CDCl_3$): δ = 7.83−7.80 (m, 2H, H_{ar}), 7.44−7.42* (m, 2H, H_{ar}), 7.32−7.28 (m, 2H, H_{ar}), 7.23−7.19* (m, 2H, H_{ar}), 7.03−6.96 (m, 1H*+1H, H_{ar}*+H_{ar}), 3.51* (s, 3H, OC**H**$_3$), 3.35 (s, 3H, OC**H**$_3$), 2.99 (s, 3H, NC**H**$_3$), 2.42* (s, 3H, NC**H**$_3$), 1.66* (s, 3H, C**H**$_3$), 1.58 (s, 3H, C**H**$_3$), 1.30 (s, 3H*+3H, C**H**$_3$*+C**H**$_3$). *main stereoisomer.

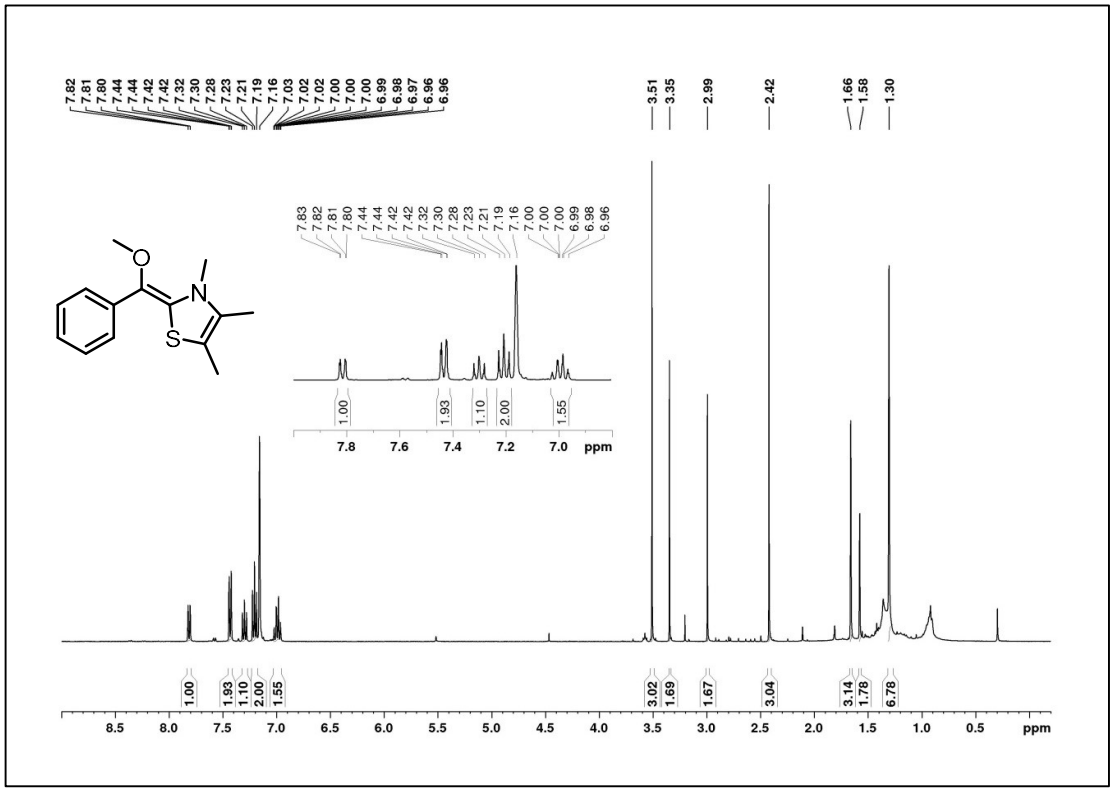

Figure SI-16. ^{1}H NMR of **OMe-EA** in C_6D_6 (400 MHz).

CV and spectro-electrochemical experiments

Cyclovoltammetry was done with an *Autolab PGSTAT302N* potentiostat (Metrohm) under Ar-atmosphere. The following electrodes have been used: glass-carbon electrode as working electrode, Pt wire as counter electrode and Ag wire as pseudo-reference electrode. Tetrabutylammonium-tetrafluoroborat served as electrolyte and ferrocene was used as an internal standard to determine the peak potentials. The samples were degassed by bubbling Ar through the solution.

Table SI-11. Summary of the measured peak potentials of **OMe-PA** and **OMe-EA** (ferrocene as reference).

	peak potential [V]			
	OMe-PA	**ferrocene**	**OMe-EA**	**ferrocene**
positive scan direction	−1.662	0.584	−1.068	0.821
	-	0.816	−0.680	0.977
	-	-	0.690	-
negative scan direction	−1.682	0.554	-	-
	0.252	0.806	-	-
	0.423	-	-	-

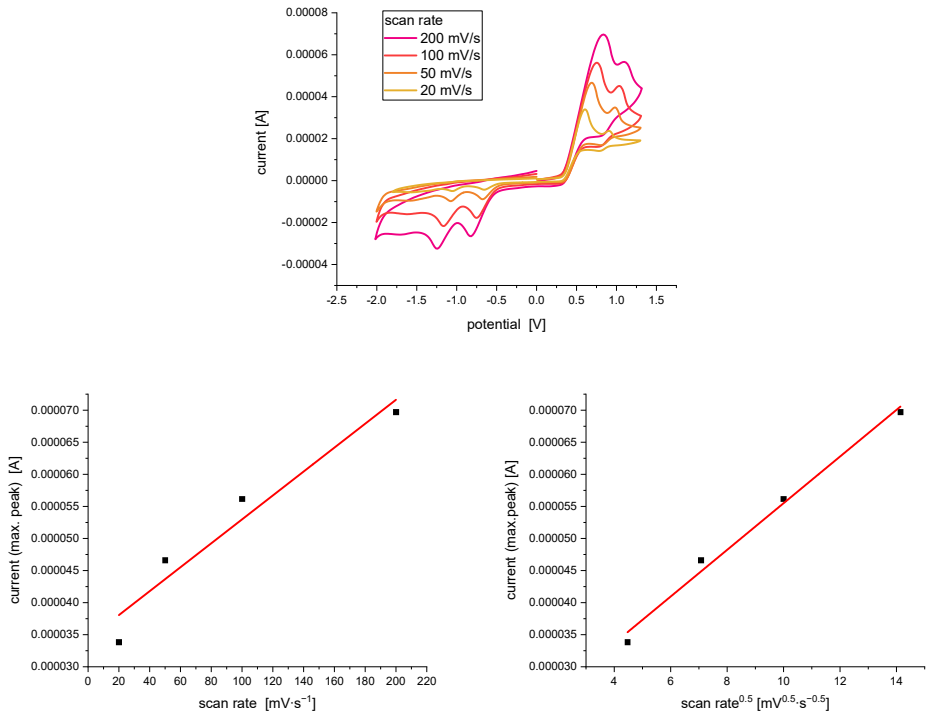

Figure SI-17. Top: Variation of scan rate: **OMe-EA** with ferrocene as reference (0.05 M in THF) Bottom left: Plot of the maximum current peaks over scan rate (linear fit with R^2 = 0.91). Bottom right: Plot of the square root of the maximum current peaks over scan rate (linear fit with R^2 = 0.99).